Acta Geologica Sinica (English Edition), 2019, 93(6): 1922–1932

Hydrogeochemical Characteristics and Groundwater Inrush Source Identification for a Multi-aquifer System in a Coal Mine

ZHANG Haitao[1, *], XU Guangquan[1, *], CHEN Xiaoqing[1], WEI Jian[2], YU Shitao[1] and YANG Tingting[1]

[1] *School of Earth and Environment, Anhui University of Science and Technology, Huainan, Anhui, 232001, China*
[2] *Geological Survey Department, Gubei Coal Mine, Huainan Mining Group, Huainan, Anhui, 232001, China*

Abstract: Correct identification of water inrush sources is particularly important to prevent and control mine water disasters. Hydrochemical analysis, Fisher discriminant analysis, and geothermal verification analysis were used to identify and verify the water sources of the multi-aquifer groundwater system in Gubei coal mine, Anhui Province, North China. Results show that hydrochemical water types of the Cenozoic top aquifer included HCO_3−Na+K−Ca, HCO_3−Na+K−Mg and HCO_3−Na+K, and this aquifer was easily distinguishable from other aquifers because of its low concentration of Na^++K^+ and Cl^-. The Cenozoic middle and bottom aquifers, the Permian fissure aquifer, and the Taiyuan and Ordovician limestone aquifers were mainly characterized by the Cl−Na+K and SO_4−Cl−Na+K or HCO_3−Cl−Na+K water types, and their hydrogeochemistries were similar. Therefore, water sources could not be identified via hydrochemical analysis. Fisher model was established based on the hydrogeochemical characteristics, and its discrimination rate was 89.19%. Fisher discrimination results were improved by combining them with the geothermal analysis results, and this combination increased the identification rate to 97.3 % and reasonably explained the reasons behind two water samples misjudgments. The methods described herein are also applicable to other mines with similar geological and hydrogeological conditions in North China.

Key words: water inrush source, multi-aquifer, hydrogeochemistry, Fisher discrimination, geothermal verification analysis, coal mine

Citation: Zhang et al., 2019. Hydrogeochemical Characteristics and Groundwater Inrush Source Identification for a Multi-aquifer System in a Coal Mine. Acta Geologica Sinica (English Edition), 93(6): 1922–1932. DOI: 10.1111/1755-6724.14299

1 Introduction

The hydrogeological conditions of coal mines in North China are extremely complicated and can seriously affect mining safety (Wu et al., 2004). In recent years, with the increase in the depth, intensity, and extent of coal mining activities groundwater disasters have gradually become more serious and hazardous. According to an officially incomplete statistical report, from 2007 to 2014, 128 water inrush accidents occurred in China, and these accidents caused serious losses to life and property (Qian et al., 2017). Over the past few years, "de-capacity" activities have ceased in many small coal mines in China, but the revival of the Silk Road is expected to promote coal mining and lead to other similar disasters (Li et al., 2015 and 2017). Therefore, understanding a site's groundwater hydrogeochemical characteristics comprehensively and identifying potential water inrush sources accurately and rapidly are of particular importance in preventing water inrush accidents.

The hydrogeochemical characteristics of groundwater can be used to identify inrush sources and predict potential mining hazards (Gavrishin et al., 2009; Wang et al., 2015; Lin et al., 2016; Li et al., 2018). At present, several methods for water inrush sources identification have been developed, and these methods cover a wide range of fields and disciplines, including in chemistry, mathematics, computer science, GIS, and statistics (Wu et al., 2014; Ma et al., 2014; Luo et al., 2016; Ma et al., 2016; Yang et al., 2016). Algorithmic mathematical models, such as fuzzy comprehensive evaluation (Gong and Jin, 2009; Wang et al., 2010; Yang et al., 2016), artificial neural network (Maier and Dandy, 1996; Kanti and Rao 2008), Bayes discriminant analysis (Hobbs, 1997; Qian et al., 2017), and Fisher discriminant analysis (Ma et al., 2014; Chen et al., 2016; Huang and Wang, 2018), yield better results than traditional discriminant methods in identifying water inrush sources. Due to its difficulty and high cost, the collection of water samples for testing tend to be limited and intermittent (Uddameri, 2007). Fisher statistics provide a more accurate and convenient means to achieve deep analysis of existing data (Martínandrés and Tejedor, 2010). Fisher discrimination has been successfully applied to many fields, such as human medical identification (Hashemipour et al., 2018), groundwater quality evaluation (Ekelund et al., 2014), and mine water source

* Corresponding author. E-mail: entao0824@163.com

identification (Ma et al., 2014; Chen et al., 2016; Huang and Wang, 2018) on account of its many advantages and feasibility.

Hydrogeochemical characteristics and water inrush source identification have been broadly studied (Shrestha and Kazama, 2007; Wu and Zhou, 2008; Ma et al., 2016; Wu et al., 2014). However, due to continuous water–rock interactions and differences in hydraulic connections between multi-aquifers, describe the overall water quality conditions by means of those methods and identification of the water inrush source correctly are difficult (Babiker et al., 2007; Stotler et al., 2009; Hu et al., 2018). Geotherms, as an important geophysical parameter, can be transmitted through a medium, such as groundwater, and changes in geotherms and groundwater temperatures through aquifer formations are continuous and equivalent (Wang and Xiong, 1991). Therefore, from a theoretical perspective, geotherms can be used to track the depth of a groundwater source or aquifer horizon and describe the physical state of the groundwater, such as its movement (Rybach and Muffler, 1981; Lee, 2006).

Due to the complexity of mine hydrogeological conditions, accurate identification of water inrush sources is challenging, and the causes of water inrush source misjudgments are often ignored. In this research, hydrochemical and Fisher discriminant analyses are used to evaluate the hydrogeochemical characteristics of the multi-aquifer groundwater system in Gubei coal mine, Anhui Province, North China and identify the related water sources. Geothermal verification analysis is then applied to verify the results of Fisher discrimination and determine the reasons behind misjudgments.

2 Study Area and Geological Setting

2.1 Study area

Gubei coal mine is located in the middle of Huainan City, Anhui Province, China (Fig. 1). It is covered with a relatively flat alluvial plain of the Huaihe River and has a total area of 34.01 km^2. The ground elevation of the mine varies from 19 m to 21 m above sea level. The mine site is situated in a temperate and semi-humid climate zone controlled by seasonal monsoons. The annual average temperature is 15.1°C and the annual precipitation is 927.30 mm. In general, the rainfall in June, July, and August accounts for approximately 40% of the total annual precipitation in the area.

2.2 Geological setting

The main strata revealed by drilling mainly include Cenozoic, Permian, Carboniferous, Ordovician, and Cambrian. The Cenozoic stratum is in nonconformity contact with the underlying Paleozoic stratum. The thickness of the Cenozoic stratum varies from 371.00 to 412.60 m, and its average thickness is 386.51m. The Permian stratum is the main coal-bearing stratum with an average thickness of 506.70 m. The claystone and sandstone layers of the Shihezi and Shanxi formations in the lower portion of the Permian stratum contain 27–42 coal beds. The Carboniferous stratum, which presents an average thickness of 113.99 m, is mainly composed of limestone, clay rock, and medium-fine sandstone; this stratum has 3–6 layers of unstable thin coalbeds. The Ordovician stratum is about 80.80-m thick and mainly composed of thick-layered dolomite and limestone. The Cambrian stratum is mainly composed of thick-layered limestone, dolomitic limestone and dolomite. Only six boreholes are exposed in this portion of the Cambrian stratum, and the exposed thickness varies from 28.5 to 442.8m.

Gubei coal mine is located in the east wing of the Chenqiao anticline. The stratigraphic strike is N10°E–N60°W with a dip direction of S80°E–S30°E. The dip angle varies from 5° to 15° and gradually decreases from shallow to deep. The main geological structures in the mine are inclined-transverse faults.

2.3 Hydrogeological setting

The main aquifers that could affect mining safety involve a loose sand pore Cenozoic aquifer group, a Permian fractured sandstone aquifer group, a Carboniferous Taiyuan Formation fractured-karst limestone aquifer group, and an Ordovician karst limestone aquifer group. According to the characteristics of the Cenozoic loose sediments and hydrogeological conditions, the Cenozoic aquifer group can be further divided into three aquifer segments. The uppermost of these segments has a thickness of 93.35–128.75 m, and the original water level of the aquifer is 7.34 m. Long-term observation data show that the water level of the aquifer fluctuates remarkably due to atmospheric precipitation and exploitation. The specific discharge of the aquifer is 0.261 –2.272 (L/s)/m, and its hydraulic conductivity and water temperature are 0.647–5.908 m/d and 18.0–19.0°C, respectively. This aquifer is mainly composed of alluvial deposits of the Huaihe River. The aquifer has good water quality and is the main source of water for the mining area.

The middle aquifer has a thickness of 173.74–247.63 m and is mainly composed of sandy clay with silt and fine-sand layers; partial intercalation with moderately coarse sand layers is also observed. The original water level of this aquifer is 12.14 m, but long-term observation data indicate that this water level is slowly decreasing. The specific discharge of the aquifer is 0.002–1.292 (L/s)/m, and its hydraulic conductivity and water temperature are 0.130–5.654 m/d and 24.0–25.2°C, respectively.

The bottom aquifer mainly consists of sand gravel and a small amount of clay; it is 40.5–88.9-m thick. The original water level of the aquifer is 6.02 m, and its natural hydraulic gradient is 1/10000. Long-term observation data show that the water level of this aquifer has dropped to 1.50 m. The specific discharge of this aquifer is 0.001–1.166 (L/s)/m, its hydraulic conductivity is 0.001–6.317 m/d, and its water temperature is 25.3–28.9°C.

The Permian fractured aquifer is distributed between the coal beds. The lithology and thickness of this aquifer vary greatly, although normally, fractures within the aquifer are not developed. The original water level of the aquifer is 23.5m below sea level (m.b.s.l.). Due to the impact of long -term mining activities, the water level of the aquifer has dropped significantly, and some local points have even

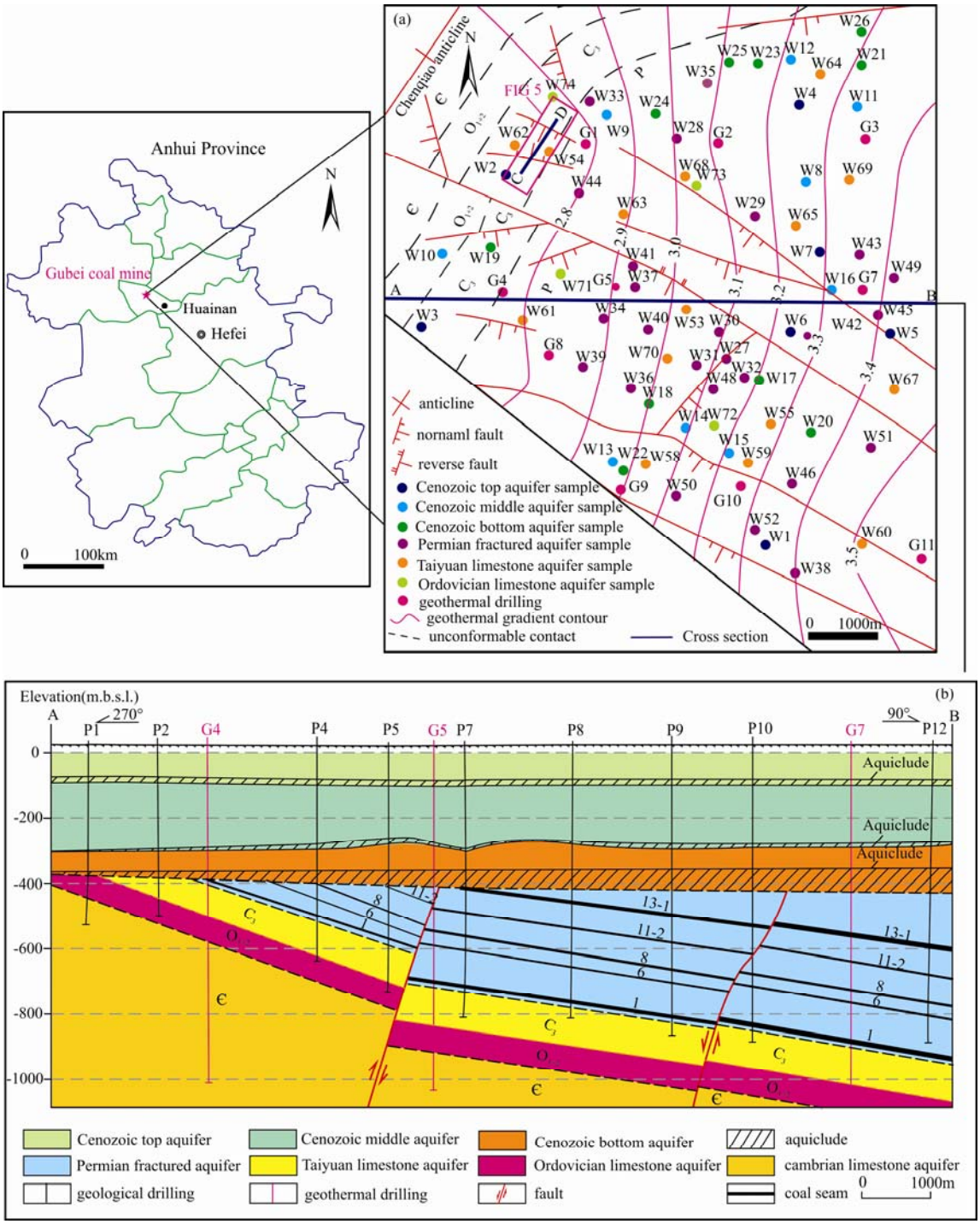

Fig. 1. Geological and hydrogeology maps of the study area.
(a) Map showing the location and the geothermal gradient contour (℃/hm) of the study area, with the distribution of water samples and geothermal drilling within Gubei coal mine; (b) Cross section of Gubei coal mine along line *A–B*.

been drained. The specific discharge of this aquifer is 0.000,05–0.003 (L/s)/m, and its hydraulic conductivity and water temperature are 0.000,4–0.016 m/d and 28.6–40.8°C, respectively.

The Taiyuan limestone aquifer is 99.99–129.11-m thick. It contains 10–13 layers of limestone, and the total thickness of limestone is 42.37–64.78 m. Twelve pumping tests show that the original water level of the aquifer ranged from 0.73 to 20.87 m. The water level of this aquifer has dropped to 6.78–235.78 m below sea level according to a long-term observation, and a cone of depression has formed around the Chenqiao anticline. The specific discharge of this aquifer is 0.0002–0.261 (L/s)/m, and its hydraulic conductivity and water temperature are 0.001–3.929 m/d and 31.0–50.0°C, respectively.

The Ordovician limestone aquifer is 52.62–86.85 m

thick. Six pumping tests show that the original water level of the aquifer is between 6.45 and 24.60 m. Its specific discharge is 0.0007–0.763 (L/s)/m, and its hydraulic conductivity and water temperature are 0.001–2.026 m/d and 32.5–41.5°C, respectively. Long-term observation data show that the water level of this aquifer has decreased locally, especially at the northern bedrock uplifting area.

3 Methods and Materials

3.1 Water samples

A total of 74 water samples were collected from the study area, including 7 from the Cenozoic top aquifer, 9 from the Cenozoic middle aquifer, 10 from the Cenozoic bottom aquifer, 26 from the Permian fractured aquifer, 18 from the Taiyuan limestone aquifer, and 4 from the Ordovician limestone aquifers. Water samples of the Permian fractured aquifer were mainly taken from mining tunnels, and the remaining water samples were taken from pumping test wells of each aquifers. The locations of the water sampling points are shown in Fig. 1.

Water temperature and pH were measured by a portable tester in the field, and Ca^{2+}, Mg^{2+}, Na^{+}, K^{+}, HCO_3^{-}, Cl^{-}, SO_4^{2-}, and TDS were measured indoors. During water sampling, samples were passed through a 0.45 μm filter and stored in a high-density polyethylene bottle. In the laboratory, SO_4^{2-} was determined by spectrophotometry; Ca^{2+}, Mg^{2+}, HCO_3^{-}, and Cl^{-} were determined by titration; and Na^{+} and K^{+} were determined by flame photometry. Since the K^{+} content in the water sample was very low, Na^{+} and K^{+} contents were summed as $Na^{+}+K^{+}$. These variables and test data were used to characterize the water quality of each aquifer and reveal the groundwater chemistry of the formation. All the water samples were in perfect charge balance with error percentages < 5%, which is acceptable. The results of water quality testing and analysis are listed in Table 1.

3.2 Geothermal data

In the study area, a total of 11 ground boreholes were used to measure geotherms, and 121 geothermal data points were obtained. The elevations of the measured geotherms were −10, −80, −180, −280, −380, −480, −580, −680, −780, −880, and −980 m. The instrument used for measurements was an HBDZ 7-1 deep-hole digital geothermal measurement recorder, the measurement range varied from −40°C to 85°C, and the measurement error was ±0.5°C. The existing geothermal data could be used to predict the spatial distribution of geotherms in the study area and verify the results of water source identification. The geothermal data for each aquifer are listed in Table 1.

3.3 Fisher discrimination

Fisher discrimination provides an optimal discriminant criterion and a solution method for the discriminant function. The main idea of Fisher discriminant analysis is to project high-dimensional data points into low-dimensional space. First, the discriminant function is established according to the distance between classes; then, the categories of the samples are determined according to the corresponding discriminant criterion (Fang, 1982; Johnson and Wichern, 2005). The discriminant function is

$$y(X) = \hat{C}_l^T X \quad l = 1, 2, 3, \cdots, m \tag{1}$$

where C_l is the eigenvector corresponding to the maximum eigenvalue and X is the independent variable matrix of the samples.

After the discriminant function is established, classification of the test object is realized by the discriminant criterion, such as the critical value method, the Mahalanobis distance method, and the new Markov distance method (Tao et al., 2013; Su et al., 2018). Among these, the Markov distance method is the most widely used. Let any sample be identified as X; the distance between the sample and the population is

$$d_t^2 = d_t^2\left(\tilde{X}, G_t\right) = \left[\hat{C}_l^T \tilde{X} - \hat{C}_l^T \tilde{X}^{(t)}\right]^T \times \left[\hat{C}_l^T \frac{W^{(t)}}{n_t - 1} \hat{C}_l^T \tilde{X}^{(t)}\right]^{-1} \left[\hat{C}_l^T \tilde{X} - \hat{C}_l^T \tilde{X}^{(t)}\right] \quad l = 1, 2, 3, \cdots, k \tag{2}$$

When $d_t^2 = \min_{l \le j \le k}\left\{d_j^2\right\}$ i.e., the distance between the sample $\tilde{X}$ and the population G_t is the minimum, and then $X \in G_t$ is judged.

In this study, the Fisher discriminant model was implemented using SPSS 19.0 to identify water inrush sources.

3.4 Geothermal analysis

A geotherm refers to the temperature of soil or a formation at different depths below the surface. Geotherms could be divided into the convection type and the conduction type based on the geological environment and heat transfer mode (Rybach and Muffler, 1981); this type of classification has been used by the international geothermal community. The conduction type of geotherms shows linear relations in the vertical direction, while the convection type shows nonlinear relations in the vertical direction (Fabbri and Trevisani, 2005). Regardless of the heat transfer types, geotherms are heterogeneous in space and may differ at the same depth or elevation (Tian et al., 2018).

In the study area, long-term monitoring data show that the geotherms have a good linear relationship with the depths or elevations in our study area (Peng et al., 2015), which demonstrates that the heat transfer mechanism is dominated by heat conduction and weakly affected by lateral convective groundwater (Fabbri and Trevisani, 2005). The linear function between the geotherm and the depth is

$$T = GH + T_0 \tag{3}$$

where G is the geothermal gradient, which refers to the increase in temperature of in the geotherm for each 100 m increase in depth and has a unit of ℃·hm^{-1}, H is the depth of the measurement point and has a unit of m, T is the geotherm at the measured depth with a unit of ℃, and T_0 is the geotherm of the constant temperature zone with a unit of ℃. According to long-term observation data in Huainan coalfield (Peng et al., 2015), the elevation of constant temperature in the study area is −10 m, and T_0 is 16.8℃. A large number of field tests show that the

Table 1 Summary statistics of groundwater variables concentrations for 74 water samples and 121 geothermal data from the six aquifers within Gubei coal mine

Aquifer ID	No. of samples	Sampling point elevation (m)	Groundwater variables concentrations								Sampling point temperature				
			Variables	Mean (mg/L)	Std. Deviation (mg/L)	Min. (mg/L)	Max. (mg/L)	Percentiles (mg/L)			Percent error (%)	Groundwater temperature (°C)	Predicted geotherm (°C)	Error (°C)	Percent error (%)
								25	50	75					
1	7	−42.5 to −72.8	Ca^{2+}	43.35	9.71	30.66	55.11	32.81	40.92	52.72	0.30 – 1.70	18.0 – 19.0	18.2 – 19.2	−0.2 – −0.1	−1.3 – −0.8
			Mg^{2+}	17.36	5.84	8.88	24.83	12.37	16.36	24.13					
			$Na^{+}+K^{+}$	144.45	51.14	73.05	206.72	104.14	126.98	201.62					
			HCO_3^{-}	448.99	15.83	425.00	466.80	432.63	448.49	463.44					
			Cl^{-}	47.38	25.69	7.52	79.99	35.00	40.41	78.34					
			$SO4^{2-}$	56.83	54.04	6.17	164.70	25.10	30.87	86.00					
			pH	7.90	0.33	7.30	8.41	7.83	7.90	8.00					
2	9	−220.7 to −295.3	Ca^{2+}	50.28	9.99	35.95	62.46	41.32	56.06	58.56	2.05 – 3.72	24.0 – 25.2	24.0 – 25.4	−0.2 – 0.2	−0.9 – 0.9
			Mg^{2+}	19.73	3.07	16.60	26.02	17.42	18.24	21.63					
			$Na^{+}+K^{+}$	804.52	26.08	767.43	843.44	777.88	803.30	826.60					
			HCO_3^{-}	268.54	57.11	160.17	330.90	222.40	292.72	303.16					
			Cl^{-}	995.92	56.21	942.53	1122.24	951.15	979.84	1023.75					
			$SO4^{2-}$	345.85	94.81	250.50	567.82	284.31	336.21	380.48					
			pH	8.34	0.13	8.18	8.59	8.26	8.31	8.45					
3	10	−312.3 to −363.4	Ca^{2+}	44.47	16.44	16.04	63.62	31.18	41.68	62.08	1.80 – 5.80	25.3 – 28.9	25.4 – 28.8	−0.2 – 0.1	−0.8 – 0.5
			Mg^{2+}	28.16	7.30	16.04	40.31	21.82	30.01	32.65					
			$Na^{+}+K^{+}$	792.14	118.23	585.26	1040.38	734.38	786.58	846.49					
			HCO_3^{-}	250.31	66.49	148.69	336.90	175.32	265.46	306.43					
			Cl^{-}	848.08	150.72	535.00	1012.90	757.58	890.05	951.65					
			$SO4^{2-}$	517.93	167.33	273.20	795.57	348.08	551.15	632.58					
			pH	8.41	0.25	7.86	8.70	8.24	8.45	8.60					
4	26	−467.1 to −715.6	Ca^{2+}	22.82	35.78	1.23	112.22	4.61	8.02	14.13	−0.76 – 3.26	28.6 – 40.8	30.2 – 41.2	−0.8 – 1.0	−1.2 – 1.1
			Mg^{2+}	12.10	20.63	0.12	62.23	0.97	1.70	9.27					
			$Na^{+}+K^{+}$	1280.43	173.13	791.90	1697.12	1196.34	1277.19	1352.82					
			HCO_3^{-}	1638.53	851.50	230.37	3097.49	824.84	2039.26	2315.76					
			Cl^{-}	576.48	188.65	213.73	957.15	462.18	524.67	612.85					
			SO_4^{2-}	399.34	575.69	1.92	1560.98	11.89	45.63	1047.05					
			pH	8.89	0.34	8.38	9.56	8.62	8.87	9.08					
5	18	−496.3 to −976.5	Ca^{2+}	26.36	15.34	8.02	48.10	12.03	24.03	40.08	−0.34 – 3.54	31.0 – 50.0	30.7 – 50.4	−1.0 – 2.5	−1.0 – 7.5
			Mg^{2+}	9.71	6.44	0.49	17.50	2.92	11.43	15.56					
			$Na^{+}+K^{+}$	1002.79	110.28	859.34	1274.02	908.78	994.67	1063.93					
			HCO_3^{-}	556.83	300.51	249.76	1419.75	341.59	420.33	787.88					
			Cl^{-}	1028.82	91.37	783.45	1212.39	988.17	1026.28	1054.64					
			SO_4^{2-}	186.85	171.99	1.23	528.33	23.54	178.67	318.87					
			pH	8.80	0.32	8.26	9.29	8.49	8.82	9.09					
6	4	−615.7 to −815.6	Ca^{2+}	30.50	20.50	8.02	49.80	10.60	32.09	48.81	0.72 – 3.76	32.5 – 41.5	34.2 – 41.8	−0.8 – 0.9	−1.2 – 0.4
			Mg^{2+}	7.21	7.96	0.36	18.15	0.88	5.17	15.59					
			$Na^{+}+K^{+}$	576.84	252.47	239.63	826.84	316.12	620.45	793.96					
			HCO_3^{-}	343.17	315.44	43.78	786.95	93.74	270.97	664.79					
			Cl^{-}	530.00	399.58	97.69	1052.06	172.53	485.12	932.35					
			SO_4^{2-}	125.65	75.55	18.45	187.32	45.96	148.42	182.58					

difference (ΔT) between the measured geotherm and the measured water temperature is less than ±1.0℃, and the error rate e% is ≤ ±1.5% within 1000m below the surface in the study area.

In this research, the universal kriging method in GIS software was used to obtain the spatial distribution of geothermal gradients based on the geothermal data of known points. This method has been widely used in the spatial analysis of edaphology, hydrology, ecology, and other fields (Isaaks and Srivastava, 1989; Christakos, 2000; Ahmadi and Sedghamiz, 2007; Nikroo et al., 2010; Wu et al., 2014; Júnez–Ferreira et al., 2016).

The universal kriging model is

$$Z(x_0)=\sum_{i=1}^{n}\lambda_i Z(x_i) \quad (4)$$

where $Z(x_0)$ is the estimated value at location x_0, λ_i is the kriging weight, and $Z(x_i)$ is the measured value at point x_i. The equation for λ_i is calculated in the same manner as presented by Ahmadi and Sedghamiz (2007).

4 Results and Discussions

4.1 Hydrogeochemical characteristics of the aquifers

A Piper trilinear diagram can be used to analyze water quality and its changing trends. As shown in Fig. 2, the water quality of the Cenozoic top aquifer is obviously different from that of the other aquifers below it. The Cenozoic top aquifer includes the HCO_3−Na+K−Ca, HCO_3−Na+K−Mg, and HCO_3−Na+K water types. The milliequivalent percentage of HCO_3^- exceeds 60% in this top aquifer, while the milliequivalent percentages of Cl^- are approximately 60% and 40%, respectively, in the Cenozoic middle and lower aquifers. The Cenozoic top aquifer is an unconfined or weakly-confined aquifer, and it directly receives low salinity water from atmospheric precipitation and surface. Therefore, the aquifer can be easily distinguished from other aquifers based on its peculiar chemistry.

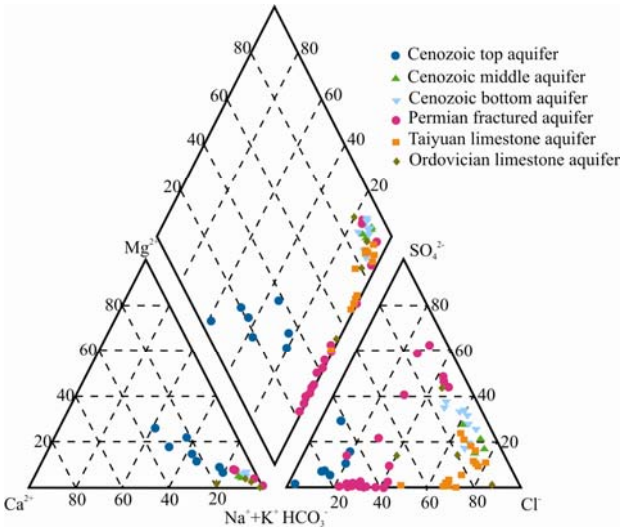

Fig. 2. Piper trilinear diagram of hydrogeochemical facies of groundwater samples from the six aquifers.

The hydrochemical types of the Cenozoic central and bottom aquifers are mostly Cl−Na+K and SO_4−Cl−Na+K. These water types are a typical feature of long-term water–rock interactions and slight surface water recharge (Qian et al., 2016 and 2018); both aquifers contain saline water. According to a previous hydrogeological survey in the mining area, a relatively stable layer of calcareous clay with an average thickness of 18.71 m developed in the lower part of the Cenozoic bottom aquifer, and this layer provides good water-proofing effects. Therefore, in the Piper trilinear diagram (Fig. 2), the water samples of the Cenozoic middle and bottom aquifers and those of the Permian fissure aquifer are rarely overlap.

As shown in Fig. 2, the water samples from the Permian fissure aquifer are dominated by alkali metal ions (Na^++K^+) relative to the concentration of alkaline earth metal ions (Ca^{2+}, Mg^{2+}), and the milliequivalent percentage of Na^++K^+ exceeds 80%. The milliequivalent percentage of HCO_3^- or SO_4^{2-} in most of the water samples from this aquifer exceeds 60%, followed by that of Cl^-. Therefore, the Permian fissure aquifer contains mainly the HCO_3−Cl−Na+K and SO_4−Cl−Na+K water types. Compared with the Cenozoic aquifer, the Taiyuan group limestone aquifer, and the Ordovician limestone aquifer, the Permian fissure aquifer samples have higher concentrations of HCO_3^- and SO_4^{2-}, which is a typical feature of pyrite oxidation and desulfurization (Liu et al., 2017; Chen et al., 2017). In its natural state, the Permian fissure aquifer is in a relatively closed environment, which causes the concentration of HCO_3^- to increase due to desulfurization. The aquifer partially changes from a closed state to a relatively open state when it affected by mining activities, which causes oxidation of pyrite in the coal seam and, eventually, an increase in concentration of SO_4^{2-}.

In the Taiyuan and Ordovician limestone aquifers, the main cations are still Na^++K^+ and the anion is mainly Cl^-, followed by HCO_3^-. The two aquifers are mainly of the Cl−Na+K and Cl−HCO_3−Na+K water types. The water samples of the Taiyuan and Ordovician limestone aquifers overlap in Fig. 2; thus, they are similar in hydrogeochemistry.

The boxplots in Figs. 3a−3f can be used to analyze the variation of ion concentrations in a multi-aquifer groundwater system. From bottom to middle to top, the box edges represent the first quartile, the median value, and the third quartile, respectively. The horizontal lines at the bottom and top of the boxplot represent the minimum and maximum values, respectively. From Figs. 3c and 3e, the Cenozoic top aquifer has a low concentration of Na^++K^+ and Cl^-; thus, this aquifer can be easily distinguished from other aquifers by these two indicators. As shown in Figs. 3a, 3c, 3d, and 3f, from the Permian fissure aquifer to the Taiyuan limestone aquifer and then to the Ordovician limestone aquifer, the concentration of Ca^{2+} shows an overall upward trend while the concentrations of Na^++K^+, HCO_3^- and SO_4^{2-} show a downward trend. This phenomenon is a typical result of carbonate dissolution and alternate cation adsorption; pyrite oxidation and desulfurization are clearly weakened (Qian et al., 2016; Chen et al., 2017).

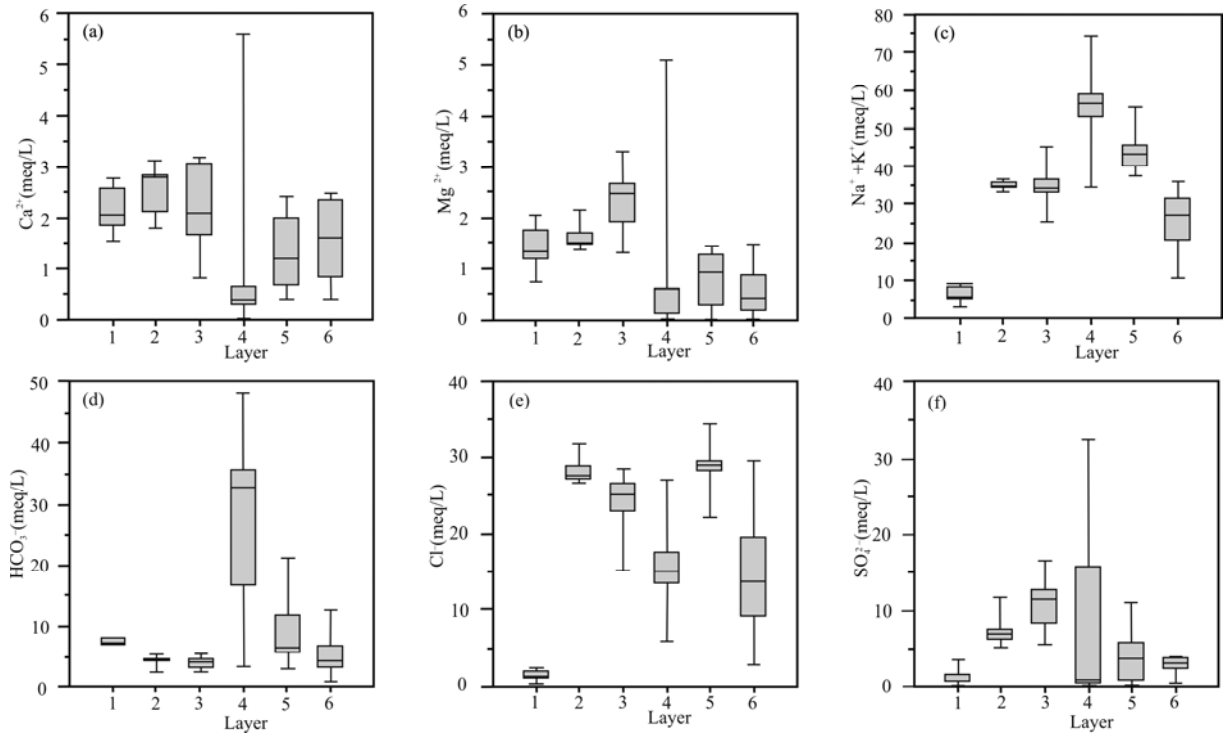

Fig. 3. Boxplots of the water samples (a-f).
Layer ID: 1-Cenozoic top aquifer; 2-Cenozoic middle aquifer; 3-Cenozoic bottom aquifer; 4-Permian fractured aquifer; 5-Taiyuan limestone aquifer; 6-Ordovician limestone aquifer.

From the above analysis, identifying the water sources of the six aquifers using only Na^++K^+, Ca^{2+}, Mg^{2+}, HCO_3^-, and SO_4^{2-} indicators is difficult. Therefore, in this research, the Fisher discriminant model was employed to identify water sources.

4.2 Fisher discriminant analysis

All of the samples were analyzed and identified by the Fisher discriminant model using SPSS 19.0. The discriminant factors were Na^++K^+, Ca^{2+}, Mg^{2+}, Cl^-, HCO_3^-, and SO_4^{2-}. Incorrect discrimination results are shown in Table 2; the remaining results are correct. The correct rate of Fisher discrimination was 89.19%, and eight water samples were misjudged. All water samples from the Cenozoic top aquifer were correctly identified. One sample (W10) from the Cenozoic middle aquifer was misjudged as being from the Cenozoic bottom aquifer, and one sample (W19) from the Cenozoic bottom aquifer was misjudged as being from the Cenozoic middle aquifer. One sample (W33) from the Permian fissure aquifer was misjudged as being from the Cenozoic bottom aquifer. Three samples (W54, W61 and W62) from the Taiyuan limestone aquifer were misjudged as belonging to the Ordovician limestone aquifer, and two water samples (W71 and W74) from the Ordovician limestone aquifer were misjudged as belonging Taiyuan formation limestone aquifer.

According to our analysis of hydrogeochemistry and regional hydrogeological conditions, the Cenozoic top aquifer is recharged by atmospheric precipitation and surface water. Therefore, this type of groundwater is characterized by obviously low TDS, low Cl^-, and high HCO_3^- and easily distinguished from other aquifers by the Fisher model.

Long-term observation data indicated the possibility of a weak hydraulic connection among the Cenozoic middle aquifer, the Cenozoic bottom aquifer, and the Permian fissure aquifer. Mining activities have caused the water

Table 2 Water samples of error identification by the Fisher discrimination

Sample no.	Elevation of water sample (m)	Aquifer ID	Discrimination result	Predicted geotherm (°C)	Measured water temperature (°C)	Difference (°C)	Percent error (%)
W10	−295.3	2	3	24.9	25	0.1	0.4
W19	−312.3	3	2	25.4	25.3	−0.1	−0.4
W33	−487.8	4	3	28.6	28.4	−0.2	−0.7
W54	−556.2	5	6	32.2	34.5	2.3	6.7
W61	−496.3	5	6	30.7	30.4	−0.3	−1.0
W62	−516.0	5	6	31.0	33.5	2.5	7.5
W71	−615.7	6	5	34.2	34.5	0.3	0.9
W74	−687.7	6	5	36.0	35.5	−0.5	−1.4

Layer ID: 1, Cenozoic top aquifer; 2, Cenozoic middle aquifer; 3, Cenozoic bottom aquifer; 4, Permian fractured aquifer; 5, Taiyuan limestone aquifer; 6, Ordovician limestone aquifer.

level of the Permian fissure aquifer to decline continuously, which would result in a gradual increase in the hydraulic gradient of the Permian fissure aquifer and the overlying Cenozoic middle and bottom aquifers. Therefore, local hydraulic connections may exist between the three aquifers, as reflected in the Piper trilinear diagram (Fig. 2), where some samples of these aquifers overlap. However, the Cenozoic middle and bottom aquifers are similar in hydrogeochemistry, which may also be related to the same lithologic (or mineral) compositions and water–rock interactions of these two aquifers. In the study area, the sediments of the Cenozoic middle and bottom aquifers contain ancient river alluvium, and cation exchange is the main hydrogeochemical action in the two aquifers (Ge, 2000; Qian et al., 2016).

At the bedrock uplifting area, the hydraulics of the Ordovician limestone aquifer and the Taiyuan limestone aquifer may be locally connected through faults, fissures, and solution fissures, which result in chemically similar groundwaters of the adjacent aquifers and changes in water temperature. This phenomenon occurs in many mines in the North China coalfield; mutual misjudgments are also frequent (Zeng et al., 2016; Qian et al., 2016; Xu et al,. 2018).

In addition, water source discriminant analysis assumes that the dataset is balanced. However, the number of water samples from the Taiyuan limestone aquifer and the Ordovician limestone aquifer (18 and 4, respectively) formed a highly unbalanced dataset (McBain and Timusk., 2011). Therefore, the results of these classifications cannot be accurately determined. Given that these aquifers are at different depths, adopting geotherms as a discriminant factor may be an efficient way to verify the results of water source discrimination.

4.3 Geothermal verification analysis

As shown in Fig. 4, a good linear relationship exists between the geotherms and the elevation ($R^2 > 0.98$), which indicates that, in the study area, the geotherm and water temperature are exchanged by means of heat conduction. Therefore, we can use equation (3) to predict the geotherm and consider the average geothermal gradient of the borehole to be the slope of the linear equation (Wang and Xiong, 1991; Peng et al., 2015). Table 3 presents the average geothermal gradient for each borehole and the results of normality tests of drilling and trend analysis. The coefficient of variation (C_v) is 28.63% –33.31% as medium variability, and the geothermal data of each borehole follow normal distribution. Therefore, universal kriging may be a suitable interpolation model for determining the geothermal gradient (Qian et al., 2017). Based on the principle of the least mean prediction error, we selected Gaussian model for the semi-variogram model to simulate geothermal gradient contours (Fig. 1) in the GIS software using the average geothermal gradient of the 11 existing boreholes. Combined with equation (3), we calculate the geotherm values corresponding to each water sampling point. The predicted geotherms and measured water temperatures of each sampling point are shown in Table 1.

In Table 1, except for the water samples of W54 and W62, the difference (ΔT) between the measured water temperatures of all other water samples and the predicted geotherms ranged from −1.0°C to 1.0°C, and e% varied from −1.3% to 1.1%; these values are within the tolerance range ($\Delta T \leq \pm 1.0$°C, $e\% \leq \pm 1.5\%$). The geothermal verification results reveal that the water samples of W10, W19, W33, W61, W71, and W74 were misjudged by the Fisher discriminant model. The correct rate of geothermal discrimination was as high as 97.30%, and only two water samples (W54 and W62) were misjudged.

The two water samples of W54 and W62 in the Taiyuan limestone aquifer were misjudged as belonging to the Ordovician limestone aquifer by Fisher model (Table 2), and their respective measured water temperatures were 2.1°C and 2.5°C higher than those predicted by the geotherms; their e% exceeded 1.5%. As seen in Fig. 1, W54 and W62 were located in the middle of a set of graben-type faults. Combining this finding with the hydrogeological conditions of the study area, we infer that the groundwater from the Ordovician and/or Cambrian limestone aquifers probably recharges the Taiyuan limestone aquifer upward (shown in Fig. 5), which causes the hydrogeochemical properties of W54 and W62 to change and their water temperature to rise. This phenomenon has been observed at many mines in the North China coalfield (Sui et al., 2011).

The above analysis revealed that geothermal verification analysis can not only verify the water source discriminant results and improve the accuracy of water source identification but also help analyze the hydraulic connections of various aquifers from the geothermal field. However, due to many other factors affecting the geothermal field, such as magmatic activity and persistent drawdown of groundwater table (Tan et al., 2009; Yin et al., 2015), identifying water sources only by comparing geotherms and groundwater temperatures is unreasonable, unscientific, and inadequate. In addition, accessing geothermal data is difficult and costly, which may limit the application of the geothermal verification in small coal mines. Therefore, other hydrogeochemical indicators, such as δD, δ^{18}O, δ^{34}S and stable isotopes (Ding et al., 2016; Rets et al., 2017; Qu et al., 2017), could be evaluated as a parameter for water source discrimination and verification in future research.

5 Conclusions

To identify water inrush sources, the factor that distinguishes various water sources was determined. Then, Fisher discriminant analysis and geothermal verification analysis were used to identify and verify the water sources of the six different aquifers. Following conclusions were derived:

Hydrochemical methods were applied to analyze the hydrogeochemial characteristics of the six aquifers in Gubei coal mine, North China. The Cenozoic top aquifer was characterized by the HCO_3−Na+K−Ca, HCO_3−Na+K−Mg and HCO_3−Na+K water types and could easily be distinguished from other aquifers. The hydrochemical types of the Cenozoic middle and bottom aquifers included Cl−Na+K and SO_4−Cl−Na+K due to

Table 3 The statistics for the geothermal data

Geothermal drilling	Geothermal gradient (°C/hm)	C_V (%)	Geotherm distribution		Model distribution	Interpolation model
			Skewness	Kurtosis		
G1	2.77	29.03	−0.09	−0.96	Normal	Universal kriging
G2	3.12	31.21	−0.03	−1.06	Normal	Universal kriging
G3	3.37	33.02	0.03	−1.19	Normal	Universal kriging
G4	2.77	28.63	0.05	−1.09	Normal	Universal kriging
G5	2.99	31.75	0.04	−1.15	Normal	Universal kriging
G6	3.12	30.34	−0.02	−1.16	Normal	Universal kriging
G7	3.38	32.52	0.12	−1.28	Normal	Universal kriging
G8	2.81	31.61	0.05	−1.12	Normal	Universal kriging
G9	2.91	31.78	0.02	−1.26	Normal	Universal kriging
G10	3.29	33.31	0.02	−1.31	Normal	Universal kriging
G11	3.52	32.44	0.36	−0.93	Normal	Universal kriging

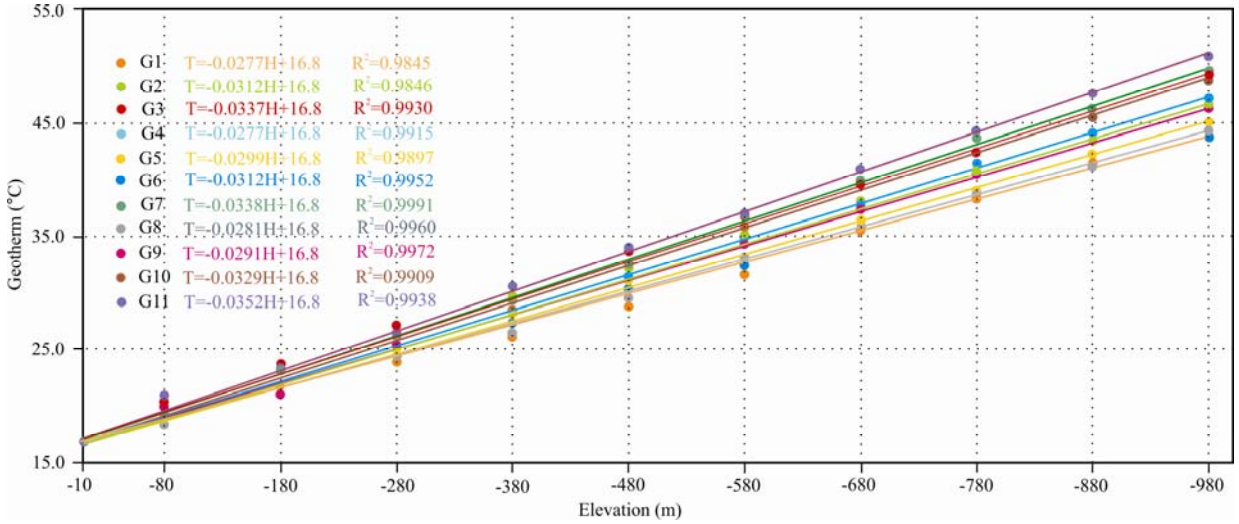

Fig. 4. Fitting curve of geotherm and elevation.
G represents geothermal drilling, amount to 11.

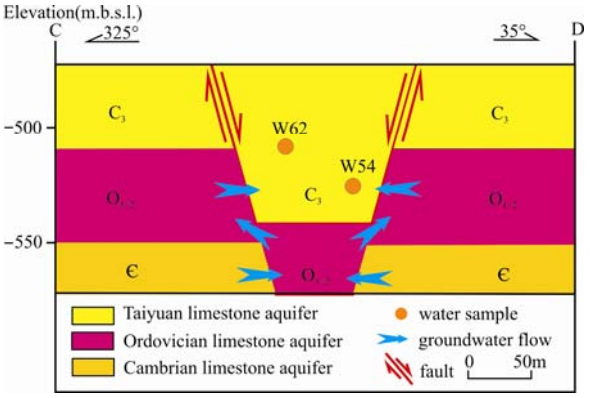

Fig. 5. Schematic cross section along line C–D.

long-term water–rock interactions and the lack of surface water recharge. The Permian fissure aquifer featured the SO_4−Cl−Na+K and HCO_3−Cl−Na+K water types because of the coexistence of pyrite oxidation and desulfurization. The hydrogeochemical types of the Taiyuan and Ordovician limestone aquifers were included the Cl−Na+K and Cl−HCO_3−Na+K water types.

(2) Except for that of the Cenozoic top aquifer, the hydrogeochemical characteristics of all other aquifers are similar. Based on hydrochemical analysis of each aquifers, we established a Fisher model to identify water sources potentially. The correct rate of Fisher discrimination was 89.19%. Through the geothermal verification analysis, it was found that six of the eight water samples misjudged by Fisher model were erroneous judgment.

(3) Based on the hydrochemical analysis and Fisher discriminant analysis, the accurate rate of geothermal verification analysis was up to 97.30%, and only two water samples were misjudged. According to the analysis, the groundwater from the Ordovician and/or Cambrian limestone aquifers probably recharged the Taiyuan limestone aquifer upward, which caused the temperature of the two water samples to be higher than the predicted temperature by more than 2.

This study will improve the theory of mine groundwater control and provide technical support for water damage prevention in the Huainan mining area. Hydrochemical analysis, Fisher discriminant analysis, and geothermal verification analysis can also be applied to accurately analyze and identify water sources for a multi-aquifer system across the entire North China coal mining region because most coal mines in North China have similar hydrogeological conditions. To extend the methods to different regions, appropriate discrimination factors (e.g., stable isotopes) must be selected for this site along with its

conditions.

Acknowledgments

This paper was financially supported by the National Natural Science Foundation of China (Grant No. 41572147). The creations and suggestions from Prof. Wu Qiang in China University of Mining and Technology (Beijing), and from Prof. Liang Xiuyu in Southern University of Science and Technology, were both appreciated. We would also like to thank those kind reviewers and editors for their considerate work before this paper publication.

Manuscript received Aug. 1, 2018
accepted Dec. 20, 2018
associate EIC HAO Ziguo
edited by LIU Lian

References

Ahmadi, S.H., and Sedghamiz, A., 2007. Geostatistical analysis of spatial and temporal variations of groundwater level. Environmental Monitoring and Assessment, 129(1–3): 277–294.

Babiker, I.S., Mohamed, A.A.M., and Hiyama, T., 2007. Assessing groundwater quality using GIS. Water Resources Management, 21(4): 699–715

Chen, L.W., Feng, X.Q., Xie, W.P., and Xu, D.Q., 2016. Prediction of water–inrush risk areas in process of mining under the unconsolidated and confined aquifer: a case study from the Qidong coal mine in China. Environmental Earth Sciences, 75(8): 706.

Chen, L.W., Xu, D.Q., Yin, X.X., Xie, W.P., and Zeng, W., 2017. Analysis on hydrochemistry and its control factors in the concealed coal mining area in North China: a case study of dominant inrush aquifers in Suxian mining area. Journal of China Coal Society, 42(4): 996–1004.

Christakos, G., 2000. Modern spatiotemporal geostatistics. New York: Oxford University Press, 304.

Ding, T.P., Gao, J.F., Tian, S.H., Wang, H.B., Li, M., Wang, C.Y., Luo, X.R., and Hang, D., 2016. Chemical and isotopic characters of the water and suspended particulate materials in the Yellow River and their geological and environmental implications. Acta Geologica Sinica (English Edition), 90(1): 285–351.

Ekelund, M., Melander, M., and Gemzell–Danielsson, K., 2014. Intrauterine contraception: attitudes, practice, and knowledge among Swedish health care providers. Contraception, 89(5): 407–412.

Fabbri, P., and Trevisani, S., 2005. Spatial distribution of temperature in the low–temperature geothermal Euganean field (NE Italy): a simulated annealing approach. Geothermics, 34(5): 617–631.

Fang, K.T., 1982. Equivalence between Fisher discriminant model and regression model. Chinese Science Bulletin, 27(8): 803–806.

Gavrishin, A.I., and Coradini, A., 2009. The origin and the formation laws of groundwater and mine water chemistry in the Eastern Donets Basin. Water Resources, 36(5): 538–547.

Ge, X.G., 2000. Sediments of the Bottom Aquifer bearing gravel of thick Cenozoic formation in Huaibei – Huainan Coalfield. Journal of China Coal Society, 25(3): 225–229 (in Chinese with English abstract).

Gong, L., and Jin, C.L., 2009. Fuzzy comprehensive evaluation for carrying capacity of regional water resources. Water Resources Management, 23(12): 2505–2513.

Hashemipour, M.A., Pourmonajemzadeh, S., Zoghitavana, S., and Navabiet, N., 2018. Relationship Between Declarations of Conflict of Interests and Reporting Positive Outcomes in Iranian Dental Journals. Science and Engineering Ethics, 2 (14): 1–11.

Hobbs, B.F., 1997. Bayesian methods for analyzing climate change and water resources uncertainties. Journal of Environmental Management, 49(4): 53–72.

Hu, S.Y., Zhao, Q.S., Wang, G.C., Zhang, J.W., and Fang, J., 2018. Hydrochemical dynamic characteristics and evolution of underground brine in the Mahai Salt Lake of the Qaidam Basin Qinghai–Tibet Plateau. Acta Geologica Sinica (English Edition), 92(5): 1981–1990.

Huang, P.H., and Wang, X.Y., 2018. Piper – PCA – Fisher recognition model of water inrush source: a case study of the Jiaozuo mining area. Geofluids, 2018: 2–10.

Isaaks, E.H., and Srivastava, R.M., 1989. An introduction to applied geostatistics. New York: Oxford University Press, 561.

Johnson, R.A., and Wichern, D.W., 2005. Applied multivariate statistical analysis. Technometrics, 47(4): 517–517.

Júnez–Ferreira, H., González, J., Reyes, E., and Herrera, G.S., 2016. A geostatistical methodology to evaluate the performance of groundwater quality monitoring networks using a vulnerability index. Mathematical Geosciences, 48(1): 25–44.

Kanti, K.M., and Rao, P.S., 2008. Prediction of bead geometry in pulsed GMA welding using back propagation neural network. Journal of Materials Processing Technology, 200(1): 300–305.

Lee, J.Y., 2006. Characteristics of ground and groundwater temperatures in a metropolitan city, Korea: considerations for geothermal heat pumps. Geosciences Journal, 10(2): 165–175.

Li, P.Y., Qian, H., and Zhou, W.F., 2017. Finding harmony between the environment and humanity: an introduction to the thematic issue of the Silk Road. Environmental Earth Sciences, 76(3): 105.

Li, P.Y., Qian, H., Howard, K.W.F., and Wu, J.H., 2015. Building a new and sustainable "Silk Road economic belt". Environmental Earth Sciences, 74(10): 7267–7270.

Li, X.X., Wu, P., Han, Z.W., Zha, X.F., Ye, H.J., and Qin, Y.J., 2018. Effects of mining activities on evolution of water quality of karst waters in Midwestern Guizhou, China: evidences from hydrochemistry and isotopic composition. Environmental Science and Pollution Research International, 25(2): 1220–1230.

Lin, M.L., Peng, W.H., and Gui, H.R., 2016. Hydrogeochemical characteristics and quality assessment of deep groundwater from the coal–bearing aquifer of the Linhuan coal–mining district, Northern Anhui Province, China. Environmental Monitoring and Assessment, 188(4): 202.

Liu, P., Hoth, N., Drebenstedt, C., Sun, Y.J., and Xu, Z.M., 2017. Hydro–geochemical paths of multi–layer groundwater system in coal mining regions – Using multivariate statistics and geochemical modeling approaches. Science of the Total Environment, 601–602: 1–14.

Luo, W.K., Shi, S.L., Lu, Y., Zou, S.H., Chen, Z.A., and Chen, L.L., 2016. Optimization study of outburst prevention measures for Tuzhu coal mine based on fixed weight clustering analysis. Journal of Geoscience and Environment Protection, 4(1): 153–161.

Ma, L., Qian, J.Z., Zhao, W.D., Curtis, Z., and Zhang, R.G., 2016. Hydrogeochemical analysis of multiple aquifers in a coal mine based on non–linear PCA and GIS. Environmental Earth Sciences, 75(8): 1–14.

Ma, R., Shi, J.S., Liu, J.C., and Gui, C.L., 2014. Combined use of multivariate statistical analysis and hydrogeochemical analysis for groundwater quality evolution: a case study in North China Plain. Journal of Earth Science, 25(3): 587–597.

Maier, H.R., and Dandy, G.C., 1996. The use of artificial neural networks for the prediction of water quality parameters. Water Resources Research, 32(32): 1013–1022.

Martínandrés, A., and Tejedor, I.H., 2010. On Conditions for Validity of the Approximations to Fisher's Exact Test. Biometrical Journal, 39(8): 935–954.

McBain, J., and Timusk, M., 2011. Feature extraction for novelty detection as applied to fault detection in machinery. Pattern Recognition Letters, 32(7): 1054–1061.

Nikroo, L., Kompani–Zare, M., Sepaskhah, A.R., and Shamsi, S.R.F., 2010. Groundwater depth and elevation interpolation by kriging methods in Mohr Basin of Fars province in Iran.

Environmental Monitoring and Assessment, 166(1–4): 387–407.
Peng, T., Wu, J.W., Ren, Z.Q., Xu, S.P., and Zhang, H.C., 2015. Distribution of terrestrial heat flow and structural control in Huainan – Huaibei Coalfield. Chinese Journal of Geophysics, 58(7): 2391–2401 (in Chinese with English abstract).
Qian, J.Z., Tong, Y., Ma, L., Zhao, W.D., Zhang, R.D., and He, X.R., 2017. Hydrochemical characteristics and groundwater source identification of a multiple aquifer system in a coal mine. Mine Water and the Environment, 37(3): 528–540.
Qian, J.Z., Wang, L., Lu, Y.H., Zhao, W.D., and Zhang, Y., 2016. Multivariate statistical analysis of water chemistry in evaluating groundwater geochemical evolution and aquifer connectivity near a large coal mine, Anhui, China. Environmental Earth Sciences, 75(9): 747.
Qian, J.Z., Zhao, W.D., Ma, L., He, X.R., Peng, Y.X., and Lu, Y.N., 2018. Hydrochemical processes and evolution of karst groundwater in the northeastern Huaibei Plain, China. Hydrogeology Journal, 26(4): 1721–1729.
Qu, S., Wang, G.C.i, Shi, Z.M., Xu, Q.Y, Guo, Y.Y., Ma, L., and Sheng, Y.Z., 2017. Using stable isotopes (δD, δ^{18}O, δ^{34}S and ^{87}Sr/^{86}Sr) to identify sources of water in abandoned mines in the Fengfeng coal mining district, Northern China. Hydrogeology Journal, 26(5): 1443–1453.
Rets, E., Chizhova, J., Loshakova, N., Tokarev, I., Kireeva, M., and Budantseva, N., 2017. Using isotope methods to study alpine headwater regions in the Northern Caucasus and Tien Shan. Frontiers of Earth Science, 11(3): 1–13.
Rybach, L., and Muffler, L.J.P., 1981. Geothermal systems: Principles and case histories. New Jersey: John Wiley and Sons, 337.
Shrestha, S., and Kazama, F., 2007. Assessment of surface water quality using multivariate statistical technique: a case study of the Fuji river basin, Japan. Environmental Modelling and Software, 22(4): 464–475.
Stotler, R.L., Frape, S.K., Ruskeeniemi, T., Ahonen, L., Onstot,t T.C., and Hobbs, M.Y., 2009. Hydrogeochemistry of groundwater in and below the base of thick permafrost at Lupin, Nunavut, Canada. Journal of Hydrology, 373(1–2): 80 –95.
Su, B., Ding, X., Liu, C., and Wu, Y., 2018. Heteroscedastic max – min distance analysis for dimensionality reduction. IEEE Transactions on Image Processing, 27(8): 4052–4065.
Sui, W.H., Liu, J.Y., Yang, S.G., Chen, Z.S., and Hu, Y.S., 2011. Hydrogeological analysis and salvage of a deep coalmine after a groundwater inrush. Environmental Earth Sciences, 62(4): 735–749.
Tan, J.Q., Ju, Y.W., Hou, Q.L., Zhang, W.Y., and Tan, Y.J., 2009. Distribution characteristics and influence factors of present geo–temperature field in Su–Lin mine area, Huaibei coalfield. Chinese Journal of Geophysics, 52(3): 732–739.
Tao, X., Lu, C., Lu, C., and Wang, Z.L., 2013. An approach to performance assessment and fault diagnosis for rotating machinery equipment. Eurasip Journal on Advances in Signal Processing, 2013(1): 5.
Tian, J., Pang, Z., Guo, Q., Wang, Y.C., Li, J., Huang, T.M., and Kong, Y.L., 2018. Geochemistry of geothermal fluids with implications on the sources of water and heat recharge to the Rekeng high – temperature geothermal system in the Eastern Himalayan Syntax. Geothermics, 74(2): 92–105.
Uddameri, V., 2007. Bayesian analysis of groundwater quality in a semi–arid coastal county of south texas. Environmental Geology, 51(6): 941–951.
Wang, J.Y., and Xiong, L.P., 1991. A new approach to identify groundwater activity by using geothermal data. Chinese Science Bulletin, 36(14): 1186–1186.
Wang, L.H., Li, G.M., Dong, Y.H., Han, D.M., and Zhang, J.Y., 2015. Using hydrogeochemical and isotopic data to determine sources of recharge and groundwater evolution in an arid region: a case study in the upper–middle reaches of the Shule River basin, northwestern China. Environmental Earth Sciences, 73(4): 1901–1915.
Wang, Y., Yang, W., Li, M., and Liu, X., 2010. Risk assessment of floor water inrush in coal mines based on secondary fuzzy comprehensive evaluation. International Journal of Rock Mechanics and Mining Sciences, 52(6): 50–55.
Wu, J., Li, P., Qian, H., Duan, Z., and Zhang, X., 2014. Using correlation and multivariate statistical analysis to identify hydrogeochemical processes affecting the major ion chemistry of waters: case study in Laoheba phosphorite mine in Sichuan, China. Arabian Journal of Geosciences, 7(10): 3973–3982.
Wu, Q., and Zhou, W.F., 2008. Prediction of groundwater inrush into coal mines from aquifers underlying the coal seams in China: vulnerability index method and its construction. Environmental Geology, 56(2): 245–254.
Wu, Q., Wang, M., and Wu, X., 2004. Investigations of groundwater bursting into coal mine seam floors from fault zones. International Journal of Rock Mechanics and Mining Sciences, 41(4): 557–571.
Wu, W.Y., Yin, S.Y., Liu, H.L., Niu, Y., and Bao, Z., 2014. The geostatisticbased spatial distribution variations of soil salts under long – term wastewater irrigation. Environmental Monitoring and Assessment, 186(10): 6747–6756.
Xu, K., Dai, G.L., and Duan, Z., 2018. Hydrogeochemical evolution of an Ordovician limestone aquifer influenced by coal mining: a case study in the Hancheng mining area, China. Mine Water and the Environment, 37(2): 238–248.
Yang, Q.F., Wang, R.J., Xu, S.N., Li, W.P., Wang, Z.Y., Mei, J.J., Ding, Z.L., and Yang, P.J., 2016. Hydrogeochemistry and stable isotopes of groundwater from Shouguang, Laizhou and Longkou in the South Coast aquifer of Laizhou Bay. Acta Geologica Sinica (English Edition), 37(5): 26–32.
Yang, W.F., Xia, X.H., Pan, B.L., Gu, C.S., and Yue, J.G., 2016. The fuzzy comprehensive evaluation of water and sand inrush risk during underground mining. Journal of Intelligent and Fuzzy Systems, 30(4): 2289–2295.
Yin, F.L., Zhang, H., and Shi, Y.L., 2015. Persistent drawdown of groundwater table in North China may reduce local climate warming rate: Numerical simulation and analysis of the impacts on shallow ground temperature. Chinese Journal of Geophysics, 58(10): 3649–3659.
Zeng, Y.F., Wu Q., Liu, S.Q., Zhai, Y.L., Zhang, W., and Liu, Y.Z., 2016. Vulnerability assessment of water bursting from Ordovician limestone into coal mines of China. Environmental Earth Sciences, 75(22): 1431.

About the first author and the corresponding author

ZHANG Haitao, male, born in 1986 in Anqing city, Anhui province; a Ph.D. student at School of Earth and Environment, Anhui University of Science and Technology. He is now interested in the study on hydrogeochemical characteristics analysis and groundwater inrush source identification. E-mail: entao0824 @163.com; phone: 13625620037.

About the corresponding author

XU Guangquan, male, born in 1967 in Lu'an city, Anhui province; a professor and doctoral supervisor at School of Earth and Environment, Anhui University of Science and Technology. He is now interested in the study on hydrogeochemical characteristics analysis and groundwater inrush source identification. E-mail: gqxu67@163.com; phone: 0554-6631118.